Title

Single-cell transcriptomics reveals aberrant skin-resident cell populations and identifies fibroblasts as a determinant in rosacea.

Permalink

Journal

Authors

Chen, Mengting

Yang, Li

Zhou, Peijie

et al.

Publication Date

DOI

Peer reviewed

Single-cell transcriptomics reveals aberrant skin-resident cell populations and identifies fibroblasts as a determinant in rosacea

Mengting Chen [1,2,3,4,11], Li Yang[1,2,3,4,11], Peijie Zhou [5,6], Suoqin Jin [7], Zheng Wu[1,2,3,4], Zixin Tan[1,2,3,4], Wenqin Xiao[1,2,3,4], San Xu[1,2,3,4], Yan Zhu[1,2,3,4], Mei Wang [1,2,3,4], Dan Jian[1,2,3,4], Fangfen Liu[1,2,3,4], Yan Tang[1,2,3,4], Zhixiang Zhao[1,2,3,4], Yingxue Huang[1,2,3,4], Wei Shi[1,2,3,4], Hongfu Xie[1,2,3,4], Qing Nie [8,9,10] ✉, Ben Wang [1,2,3,4] ✉, Zhili Deng [1,2,3,4] ✉ & Ji Li [1,2,3,4] ✉

Rosacea is a chronic inflammatory skin disorder, whose underlying cellular and molecular mechanisms remain obscure. Here, we generate a single-cell atlas of facial skin from female rosacea patients and healthy individuals. Among keratinocytes, a subpopulation characterized by IFNγ-mediated barrier function damage is found to be unique to rosacea lesions. Blocking IFNγ signaling alleviates rosacea-like phenotypes and skin barrier damage in mice. The papulopustular rosacea is featured by expansion of pro-inflammatory fibroblasts, Schwann, endothelial and macrophage/dendritic cells. The frequencies of type 1/17 and skin-resident memory T cells are increased, and vascular mural cells are characterized by activation of inflammatory pathways and impaired muscle contraction function in rosacea. Most importantly, fibroblasts are identified as the leading cell type producing pro-inflammatory and vasodilative signals in rosacea. Depletion of fibroblasts or knockdown of PTGDS, a gene specifically upregulated in fibroblasts, blocks rosacea development in mice. Our study provides a comprehensive understanding of the aberrant alterations of skin-resident cell populations and identifies fibroblasts as a key determinant in rosacea development.

Rosacea is a commonly chronic inflammatory skin disorder that mainly affects the central face. The prevalence has been estimated to range from less than 1 to 22% across populations worldwide[1–3]. Rosacea is characterized by facial erythema, telangiectasia, edema, papules, pustules and recurrent flushing. According to the clinical features, it is classified into four subtypes, including erythematotelangiectatic (ETR),

papulopustular (PPR), phymatous (PhR), and ocular rosacea, although there may be overlaps between different subtypes[4,5]. The pathogenesis involves damaged skin barrier, dysregulated inflammatory responses (perivascular or pilosebaceous infiltration), hyperactive neurovascular reactivity (dilation), glandular hyperplasia and fibrotic changes[6–11], a composition reflecting the multivariate process of this disease.

[1]Department of Dermatology, Xiangya Hospital, Central South University, Changsha, Hunan, China. [2]Hunan Key Laboratory of Aging Biology, Xiangya Hospital, Central South University, Changsha, Hunan, China. [3]National Clinical Research Center for Geriatric Disorders, Xiangya Hospital, Central South University, Changsha, Hunan, China. [4]FuRong Laboratory, Changsha, China. [5]Center for Machine Learning Research, Peking University, Beijing, China. [6]AI for Science Institute, Beijing, China. [7]School of Mathematics and Statistics, Wuhan University, Wuhan, China. [8]Department of Mathematics, University of California Irvine, Irvine, CA, USA. [9]The NSF-Simons Center for Multiscale Cell Fate Research, University of California Irvine, Irvine, CA, USA. [10]Department of Developmental and Cell Biology, University of California Irvine, Irvine, CA, USA. [11]These authors contributed equally: Mengting Chen, Li Yang. ✉e-mail: qnie@uci.edu; wangben@csu.edu.cn; dengzhili@csu.edu.cn; liji_xy@csu.edu.cn

To date, existing concepts regarding the pathophysiology of rosacea have been obscure and mainly limited to histomorphology, global gene analysis and immunohistochemistry due to the fact that laboratory models are not fully representative of rosacea[7,12–16]. Single-cell RNA-sequencing (scRNA-seq) has emerged as a powerful tool to define the cellular composition (including novel or rare cell sub-populations), cell-specific transcriptome dynamics, cell lineage tracing and cell-cell communications in complex tissues at uniquely high resolution[17–20]. However, to our knowledge, a study regarding scRNA-seq application for investigating the pathogenesis of rosacea has never been reported.

Here, we report scRNA-seq analysis for 131,243 cells from 3 conditions: lesional and non-lesional facial skin from female rosacea patients, and facial skin from female healthy individuals. Via single-cell-level resolution, we provide an atlas of the complexity and diversity of aberrant skin-resident cell populations in rosacea. Most importantly, by combining cell-cell communication analysis with mouse model assays, we identify fibroblasts as a key determinant in the pathogenesis of rosacea, suggesting an important role for mesenchymal sub-populations in the treatment of inflammatory skin disorders.

Results

scRNA-seq atlas of cell populations in rosacea

We obtained skin biopsies from lesional and non-lesional facial skin of 9 female rosacea patients (including 3 ETR, 3 PPR and 3 PhR) and facial skin of 3 female healthy individuals. To dissect the cellular and molecular changes in rosacea, we performed scRNA-seq on these skin biopsies from the seven conditions: facial skin from healthy individuals (HS), non-lesional and lesional facial skin from ETR patients (ETR_N and ETR_L), non-lesional and lesional facial skin from PPR patients (PPR_N and PPR_L), non-lesional and lesional facial skin from PhR patients (PhR_N and PhR_L) (Fig. 1a). After quality control ("Methods"), 131,243 cells were reserved for subsequent analyses. Using the integration methods from Seurat R package, total 28 clusters (c0-c27) were obtained, which were distinguished by distinct marker genes (Supplementary Fig. 1a). These clusters could be reproduced with cells from each of the 21 samples, suggesting that they are robustly present across different samples and conditions (including HS, ETR_N, ETR_L, PPR_N, PPR_L, PhR_N and PhR_L) (Supplementary Fig. 1b, c).

The above 28 clusters were further identified as 11 different cell types, based on the expression of known markers, including keratinocytes (KRT14+, KRT10+), fibroblasts (DCN+, PDGFRA+), Schwann cells (MPZ+, MBP+), endothelial cells (VWF+, PECAM1+), vascular mural cells (vMCs) (ACTA2+, MYL9+), T cells (CD3D+, CD3E+), macrophages/dendritic cells (DCs) (AIF1+), melanocytes (PMEL+), sweat gland cells (AQP5+), B cells (CD79A+), mast cells (TPSB2+)[21–25] (Supplementary Fig. 2; Fig. 1b–d; Supplementary Data 1; Supplementary Fig. 3a–e). We defined the relative proportion of each cell type in all samples, showing significant alterations in cellular composition in rosacea skin compared with HS (Fig. 1e; Supplementary Data 2 and 3). The immune cell infiltrations were made up of T cells, macrophages/dendritic cells, mast cells and B cells in the lesional skin of rosacea patients. Thereinto, T cells were the dominant infiltrating cells, and increased in the lesional skin of all rosacea subtypes, even in the non-lesional skin of PPR and PhR (HS: 1.398%, ETR_N: 1.586%, ETR_L: 5.767%, PPR_N: 7.536%, PPR_L: 36.241%, PhR_N: 3.97%, PhR_L: 8.682%); macrophages/dendritic cells were significantly increased in the lesional skin of PPR, and slightly increased in the lesional skin of ETR and PhR (HS: 1.058%, ETR_N: 0.8%, ETR_L: 1.742%, PPR_N: 1.695%, PPR_L: 2.03%, PhR_N: 1.27%, PhR_L: 1.833%); the proportions of mast cells showed no significant changes; while B cells were mainly increased in the lesional skin of PPR (HS: 0.023%, ETR_N: 0.029%, ETR_L: 0.119%, PPR_N: 0.0365%, PPR_L: 1.749%, PhR_N: 0.019%, PhR_L: 0.219%) (Fig. 1f; Supplementary Fig. 3f). Only PPR skin displayed a slight increase in the proportion of fibroblasts. Endothelial cells were obviously increased in PPR and slightly increased in PhR (HS: 0.387%, ETR_N: 0.143%, ETR_L: 0.415%, PPR_N: 1.14%, PPR_L: 3.327%, PhR_N: 0.234%, PhR_L: 4.202%) (Fig. 1f). Due to the increase in inflammatory cell infiltrations, keratinocytes were decreased in the lesional skin of all rosacea types, even in the non-lesional skin of PPR (HS: 93.82%, ETR_N: 92.50%, ETR_L: 87.36%, PPR_N: 72.31%, PPR_L: 43.90%, PhR_N: 89.58%, PhR_L: 79.56%) (Fig. 1f). However, the proportions of other cells, including vascular mural cells, Schwann cells, melanocytes and sweat gland cells, showed no remarkable alterations (Supplementary Fig. 3f). Since the healthy skin samples were dominated by epidermal cells, this caveat should be kept in mind regarding all conclusions for cellular proportion (especially for fibroblasts). Taken together, these results reveal the composition and alterations of cell populations in rosacea skin.

Identification of keratinocyte subpopulations in rosacea

Keratinocytes, the most dominant cell type in the epidermis of skin, have been demonstrated to participate in the pathogenesis of multiple inflammatory skin disorders, such as psoriasis and atopic dermatitis[26]. Here, by performing subclustering analysis, keratinocytes were separated into 14 subclusters (Supplementary Fig. 4a). According to the structure of human skin and the expression of known markers[27,28], the above clusters were further identified as 4 classical subpopulations, including basal stem (KRT15+), mitotic (MKI67+), spinous (KRT1+, KRT10+), and granular (FLG+, LOR+) keratinocytes (Fig. 2a; Supplementary Fig. 4b, c; Supplementary Data 4). In addition, we unexpectedly found a keratinocyte subpopulation with high expression of CD74, which was mainly expanded in the lesional skin of PPR, and slightly increased in ETR and PhR (Fig. 2a–d; Supplementary Fig. 4b; Supplementary Data 4). By immunostaining, we confirmed the expansion of CD74+ keratinocytes in the lesional epidermis of all rosacea types (Fig. 2e, f).

To determine the differences in CD74+ keratinocytes between lesional and healthy or non-lesional skin, we performed Gene Set Enrichment Analysis (GSEA) using both Gene Ontology (GO) and Kyoto Encyclopedia of Genes and Genomes (KEGG) terms. Our results showed that in CD74+ keratinocytes of lesional skin, interferon (IFN) related pathways were significantly upregulated, whereas skin barrier-related pathways, such as tight junction, adherens junction and cell adhesion molecules, were significantly downregulated (Fig. 2g, h). Notably, the identified skin barrier damage in rosacea was characterized by the downregulation of multiple claudins (CLDNs) (Fig. 2i), consistent with our previous report[8]. The hyperactivation of IFN signaling pathway was further supported by the upregulation of multiple IFN-related genes and by immunostaining of IRF1 and p-STAT1, two active downstream proteins of IFN signaling pathway[29] (Fig. 2j–l; Supplementary Fig. 4d, e).

Previous studies have linked IFN signaling to epidermal barrier function and the pathogenesis of various inflammatory skin diseases[30–33]. However, the functional role of IFN signaling in rosacea remains largely unknown. We first analyzed the expression of type I interferons, including IFNα (IFNA1, IFNA2, IFNA4, IFNA5, IFNA6, IFNA7, IFNA8, IFNA10, IFNA13, IFNA14, IFNA16, IFNA17 and IFNA21), IFNβ (IFNB1), IFNω (IFNW1), IFNε (IFNE), IFNκ (IFNK), and type II interferon (IFNG) in our scRNA-seq datasets. Our results showed that none of the type I interferons was detected, but type II interferon (IFNG) was obviously and specifically expressed in T cells and upregulated in the lesional skin of different rosacea subtypes (Supplementary Fig. 5a–g). These results were further confirmed by our previously published bulk RNA-seq datasets[34] (Supplementary Data 5; Supplementary Fig. 5h). Furthermore, we analyzed the expression of type I IFN receptors (IFNAR1 and IFNAR2) and type II IFN receptors (IFNGR1 and IFNGR2), and showed that both type IFN receptors were expressed in the facial skin, and type II IFN receptors were robustly expressed in epidermal keratinocytes (Supplementary Fig. 5i, j). All the above results suggest an important role of IFN gamma (IFNγ) signaling in rosacea. To this
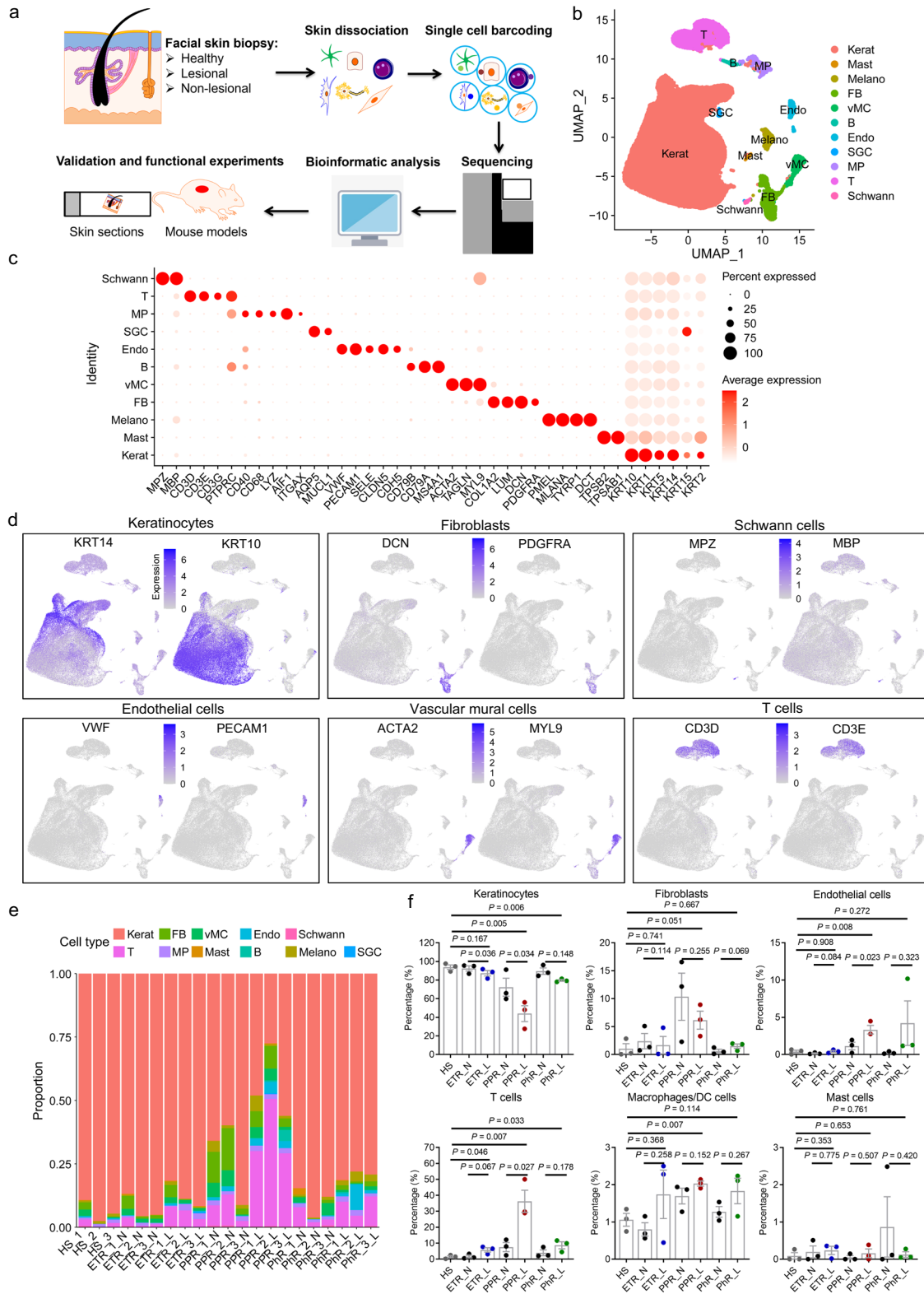
end, we first generated a cathelicidin LL37-induced rosacea-like mouse model, which resembles the clinical symptoms of rosacea patients in accordance with previous studies[10,16]. By co-immunostaining of CD4 and IFNγ, we further confirmed that IFNγ was mainly expressed and upregulated in the T cells of lesional skin of rosacea-like mouse model (Supplementary Fig. 6a, b). Then, IFNγ neutralizing antibodies were

subcutaneously injected to investigate the functional role of IFNγ signaling in the development of rosacea (Supplementary Fig. 7a). As expected, neutralizing antibody injection significantly inhibited the activation of IFNγ signaling and obviously alleviated the rosacea-like phenotypes in mice (Supplementary Fig. 7b, c; Fig. 2m, n). The dermal infiltrating cells and rosacea-associated gene expression were also

Fig. 1 | scRNA-seq reveals cell type composition in skin lesions of rosacea patients and healthy individuals. a Flowchart overview of scRNA-seq, and subsequent validation and functional experiments. Skin biopsies from the seven conditions: facial skin from healthy individuals (HS), non-lesional and lesional facial skin from ETR patients (ETR_N and ETR_L), non-lesional and lesional facial skin from PPR patients (PPR_N and PPR_L), non-lesional and lesional facial skin from PhR patients (PhR_N and PhR_L). **b** Uniform manifold approximation and projection (UMAP) plot showing the 11 cell types of human facial skin. Kerat, keratinocyte; Mast, mast cell; Melano, melanocytes; FB, fibroblast; vMC, vascular mural cell; B, B cell; Endo, endothelial cell; SGC, sweat gland cell; MP, macrophage/DCs; T, T cell; Schwann, Schwann cell. **c** Dot plot showing the expression of marker genes of each cell type. **d** Feature

plots showing expression of marker genes for the keratinocytes (KRT14, KRT10), fibroblasts (DCN, PDGFRA), Schwann cells (MPZ, MBP), endothelial cells (VWF, PECAM1), vMCs (ACTA2, MYL9), T cells (CD3D, CD3E). **e** Bar graph showing the proportion of major cell type populations of each sample. HS_1, facial skin from healthy individual 1. ETR_1_N, non-lesional facial skin from ETR patient 1. ETR_1_L, lesional facial skin from ETR patient 1. PPR_1_N, non-lesional facial skin from PPR patient 1. PPR_1_L, lesional facial skin from PPR patient 1. PhR_1_N, non-lesional facial skin from PhR patient 1. PhR_1_L, lesional facial skin from PhR patient 1. **f** The percentage of different cell types in different conditions ($n = 3$ samples for each group from scRNA-seq datasets). The data represent the means ± SEM. *P*-values were determined by two-tailed unpaired (L vs HS) or paired (L vs N) Student's *t*-test.

improved (Supplementary Fig. 7d; Fig. 2o, p). Moreover, we found that neutralization of IFNγ not only inhibited the expansion of CD74^{+} keratinocytes (Supplementary Fig. 7e, f) but also restored the expression of multiple epidermal barrier genes (mainly CLDNs) and transepidermal water loss (TEWL) in LL37-induced mice skin (Fig. 2q–t; Supplementary Fig. 7g). Consistently, the expression of epidermal barrier genes, including CLDNs and tight junction proteins (TJPs), was impaired in IFNγ-treated human keratinocytes in vitro (Supplementary Fig. 7h). Collectively, these results identify a disease-enriched keratinocyte subpopulation with hyperactivation of IFNγ signaling, which may be responsible for the skin barrier damage and pathogenesis of rosacea.

Identification of fibroblast subpopulations in rosacea
Fibroblasts are the main cell type in the dermis, which have been reported to play different roles in the pathogenesis of inflammatory diseases[35]. However, the functional role of fibroblasts in rosacea development is unknown. In this study, by performing subclustering analysis, fibroblasts were separated into 10 subclusters (Supplementary Fig. 8a). Hierarchical cluster analysis demonstrated that fibroblasts could further be divided into 5 subpopulations, referred to as complement C3[+] (C3[+]), IGFBP3^{+}, SFRP2^{+}, ASPN[+], and DSG1^{+} fibroblasts according to their specific markers respectively. Among these, C3[+] fibroblasts were found to be unique to the lesional skin of PPR rosacea (Supplementary Fig. 8b–e; Fig. 3a–d; Supplementary Data 6). Considering HS_2 and HS_3 samples were dominated by epidermal cells, and only 4 and 9 fibroblast cells were collected respectively (Supplementary Data 3), this caveat should be kept in mind regarding the proportion of fibroblasts. By co-immunostaining of C3 and DCN, a marker of fibroblasts[21] (Fig. 1d), we verified the significant expansion of C3[+] fibroblasts in the lesional skin of PPR patients and revealed a slight increase in ETR and PhR lesional skin (Fig. 3e, f).

To figure out the potential role of C3[+] fibroblasts in the pathogenesis of rosacea, we conducted Gene Set Enrichment Analysis (GSEA) by using the marker genes (Supplementary Data 6). Our results showed that the upregulated pathways were mainly associated with inflammation, such as chemokine signaling pathway, cytokine-cytokine receptor interaction, TNF signaling pathway and NF-kappa B signaling pathway, suggesting an apparent pro-inflammatory role for C3[+] fibroblasts (Fig. 3g). Consistently, a series of chemokines, including *CCL19, CXCL1, CXCL2* and *CXCL12*, was demonstrated to be highly expressed in C3[+] fibroblasts in the lesional skin of PPR patients (Fig. 3h, i; Supplementary Data 6). More importantly, we demonstrated that these chemokines (*CCL19, CXCL1, CXCL2* and *CXCL12*) were basically expressed in C3[+] fibroblasts across all cell types of the whole skin (Supplementary Fig. 8f; Fig. 3j), suggesting they are fibroblast-specific chemokines in rosacea skin lesions. IFNγ neutralization decreased the expression of CCL19 in the fibroblasts of LL37-induced mice skin (Supplementary Fig. 8g, h). Collectively, these results reveal that fibroblasts contribute to the amplification of inflammation through transition to a pro-inflammatory state in the pathogenesis of rosacea.

Identification of Schwann cell subpopulations in rosacea
Numerous lines of evidence suggest a key role of neurogenic inflammation in rosacea development[11,36–39]. Although any type of neuron cell was not found in our scRNA-seq datasets, we identified a cluster of Schwann cells, the major glial cell type in the peripheral nervous system. By performing subclustering analysis, Schwann cells were separated into 2 subclusters (Supplementary Fig. 9a, b; Supplementary Data 7). Among these, a CD74^{+} subpopulation was found to be remarkably expanded in the lesional skin of PPR patients (Supplementary Fig. 9c–e), which was further confirmed by co-immunostaining of CD74 and MBP (Supplementary Fig. 9f, g); and the sample sizes are too small to know if other rosacea subtypes have similar findings. However, these CD74^{+} Schwann cells were not found in LL37-induced rosacea-like mice skin (Supplementary Fig. 9h).

To illustrate the potential role of Schwann cells in the development of rosacea, we performed GSEA. Our results demonstrated that the upregulated pathways were primarily involved in inflammation, such as IL-17 signaling pathway, inflammatory mediator regulation of TRP channels, Toll-like receptor signaling pathway and antigen processing and presentation (Supplementary Fig. 9i), suggesting Schwann cells receive more inflammatory signals, which may play a role in the pathogenesis of rosacea.

Changes in different immune cell populations in rosacea
Dysregulation of the immune system is the hallmark of rosacea[9], but the changes in immune cells at the single-cell level have not been defined. As described above, our results showed that T cells are the dominant infiltrating cells, and macrophages/DCs and B cells are also increased in the lesional skin of rosacea, especially in PPR (Fig. 1e, f; Supplementary Fig. 3f; Supplementary Data 2 and 3). To investigate the changes of T cells in rosacea, we first analyzed the transcriptional profile, and found that multiple inflammation-associated genes, including S100As, IFNG and CCL5[40–42], were upregulated in T cells in the lesional skin of all subtypes of rosacea (Supplementary Fig. 10a). Next, we integrated T cells from all samples and yielded 7 subclusters (T_c0 to T_c6) according to the previously described strategies[25], among which T_c1 is CD8 positive while others are CD4 positive cells (Fig. 4a; Supplementary Fig. 10b). Detailedly, T_c0 (highly expressed Th1 marker genes, *IFNG* and *TBX21*[43]) and T_c2 (highly expressed Th17 marker genes, *IL17A* and *RORC*[44]) were obviously increased in the lesional skin of PPR patients, and slightly expanded in certain ETR or PhR patients; T_c6 (expressed Th2 marker gene, *IL13*[45]) was also slightly increased. Compared with HS and N skin, T_c4 (highly expressed Treg marker genes, *FOXP3* and *IL2RA*[46]) showed an increase in the lesional skin of PPR and PhR patients (Fig. 4b–d). Notably, we found that T_c3 (highly expressed TRM marker gene, *ITGAE*[21]) was mildly expanded in rosacea (Fig. 4b–d), which was confirmed by the co-immunostaining of CD69 and CD103, two typical markers of TRM cells[21] (Fig. 4e, f).

Macrophages/DCs were separated into 1 macrophage and 3 DC (DC1, DC2 and DC3) populations (Fig. 4g). Among these, macrophages were identified by expression of *CD68, ITGAM* and *FCGR1A* (Supplementary Fig. 10c). Although all DCs expressed AIF1 (Supplementary
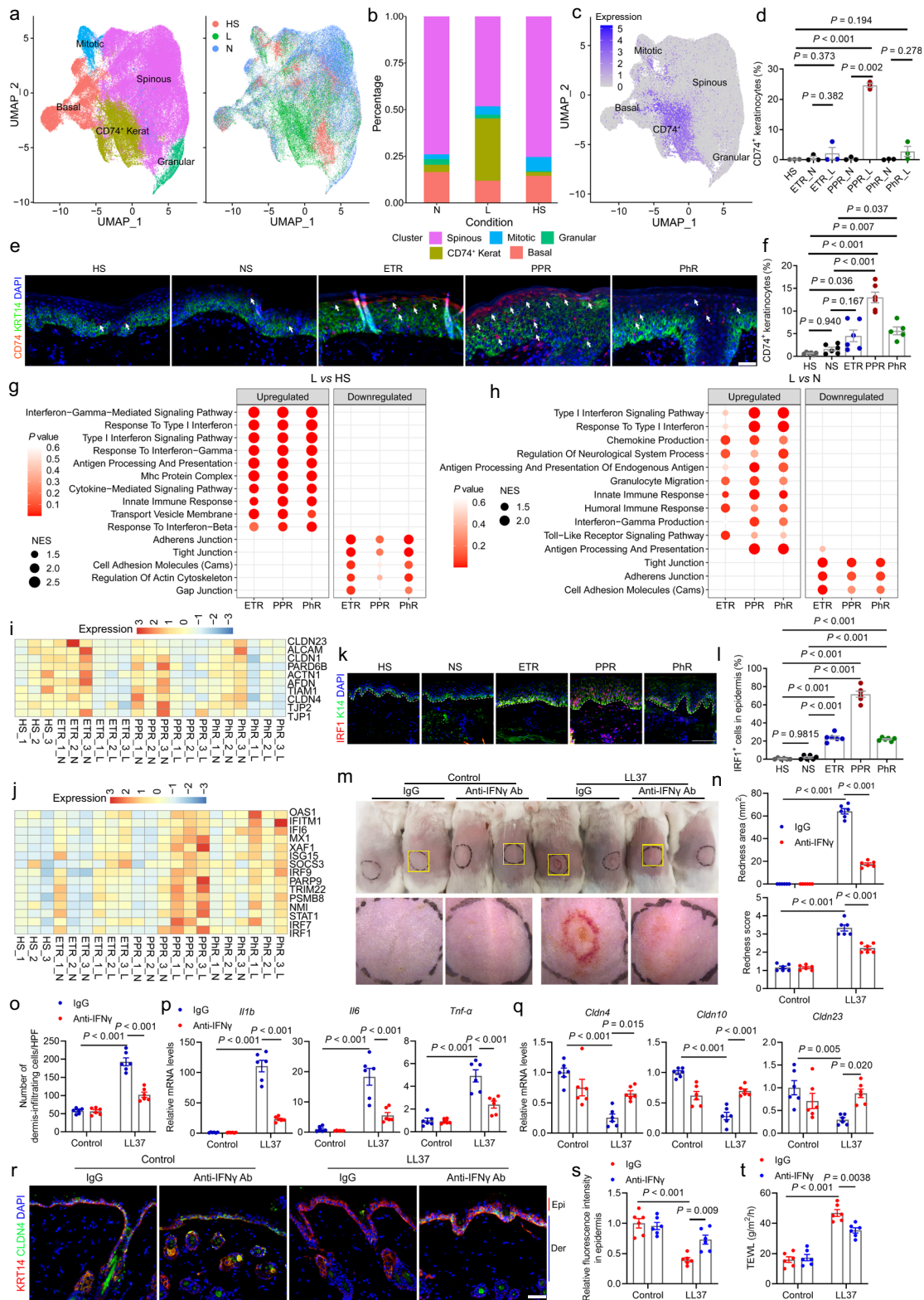
Fig. 3a), DC1 and DC3 were characterized by higher expression of *CD1A* and *FCER1A* (Supplementary Fig. 10d). Compared with HS and N skin, the percentage of macrophages was significantly expanded in the lesional skin of PPR and slightly increased in ETR and PhR, while DCs showed no obvious alteration in rosacea (Fig. 4h, i; Supplementary Fig. 10e, f). To uncover the transcriptional changes of macrophages between lesional skin and HS/N, we performed differentially expressed genes (DEGs) analysis and found that multiple chemokines (including CCL5, CXCL9, CXCL10, CXCL11, CXCL12) involved in T cell activation and differentiation were increased in the lesional skin of PPR patients (Fig. 4j). CXCL10+ macrophages were also increased in rosacea mouse model, which was restored by IFNγ neutralization (Supplementary Fig. 10g, h). Further GSEA analysis showed that complement and coagulation cascades, antigen processing and presentation, Toll-like receptor signaling pathway related to immune response were commonly upregulated in macrophages of all subtypes of rosacea (Fig. 4k).

Fig. 2 | Identification of keratinocyte subpopulations in rosacea. a UMAP plots showing keratinocyte subclusters and sample conditions. **b** Bar graph showing subpopulation percentage. **c** Feature plot showing CD74 expression in keratinocytes. **d** The percentage of CD74⁺ keratinocytes ($n = 3$ samples for each group). **e** Immunohistochemistry of KRT14, CD74 in HS, normal skin of patients (NS), and lesional skin of ETR, PPR, PhR. White arrows indicate CD74⁺ keratinocytes. Scale bar, 50 μm. **f** Quantification of CD74⁺ keratinocytes ($n = 6/6/6/6/5$ samples for HS/NS/ETR/PPR/PhR group used in **e**). **g, h** Top-ranked enriched pathways in CD74⁺ keratinocytes of L versus HS (**g**), L versus N (**h**). NES indicates enrichment scores. The color keys from red to blue indicate the P-value range. Two-sided permutation test without multiple comparison adjustments was used. **i** Heatmap of skin barrier-related genes in CD74⁺ keratinocytes. **j** Heatmap of IFN-related genes in CD74⁺ keratinocytes. **k** Immunohistochemistry of IRF1, KRT14. Scale bar, 100 μm. **l** Quantification of IRF1⁺ keratinocytes in epidermis $n = 6/6/6/6/5$ samples for HS/NS/ETR/PPR/PhR group used in **k**). **m** The back skins of IgG and anti-IFNγ antibody-treated mice intradermally injected with LL37 or control vehicle. Images were acquired 48 h after the first LL37 injection. Below panels, magnified images of yellow boxed areas. **n** The severity of the rosacea-like symptoms was determined with the redness area and score ($n = 6$). **o** Dermal infiltrating cells were quantified ($n = 6$). **p** The relative mRNA levels of *Il1β, Il6, Tnfα* in mice skins ($n = 6$). **q** The relative mRNA levels of *Cldn4, Cldn10, Cldn23* in mice skins ($n = 6$). **r** Immunohistochemistry of CLDN4, KRT14 in mice skins. Scale bar, 50 μm. Epi, Epidermis. Der, Dermis. **s** Quantification of relative fluorescence intensity for CLDN4 in epidermis ($n = 6$). **t** Quantification of TEWL ($n = 6$). All results are representative of at least three independent experiments. Data are presented as mean ± SEM, and P-values were determined by one-way ANOVA with Tukey's post hoc test (**f, l, n, o, p, q, s, t**) and two-tailed unpaired (L vs HS) or paired (L vs N) Student's t-test (**d**).

Collectively, these results suggest that Th1/Th17 polarization and macrophage infiltration are the hallmarks of skin inflammation, and resident memory T cells may play an underestimated role in rosacea.

Alterations in vascular cell populations in rosacea

Besides inflammation, vascular dysfunction, such as vasodilation, is another hallmark of rosacea[1]. However, the cellular and molecular changes in cells of blood vessel structures remain obscure. We first analyzed vascular mural cells (vMCs), including vascular smooth muscle cells (vSMCs) and pericytes, which are responsible for the contraction and relaxation of vascular vessels[47–50]. First, according to previous study[21], pericytes were distinguished from vSMCs by RGS5, a marker for pericytes (Supplementary Fig. 11a, b). By performing subclustering analysis, vSMCs were separated into 2 subclusters, but the percentage and distribution of subclusters were comparable across HS, N and L, suggesting that vSMC cell identity may not alter in rosacea (Supplementary Fig. 11c, d; Supplementary Data 8). To discover the potential changes of vSMCs in rosacea, we performed GSEA analysis and found that multiple pathways involved in inflammatory responses were routinely upregulated in vSMCs, such as IL-17 signaling pathway (Supplementary Fig. 11e, f). Pericytes were separated into 2 subclusters, whose percentage and distribution were also not affected in rosacea (Supplementary Fig. 11g, h; Supplementary Data 9). Similar to vSMCs, several inflammatory pathways were activated in pericytes, including IL-17 signaling pathway and NF-Kappa B signaling pathway (Supplementary Fig. 11i). Although alterations in muscle contraction function were not identified in our scRNA-seq datasets, we detected the contractile activity of vMCs by co-immunostaining of α-SMA (a vMC marker) and phosphorylated myosin light chain 2 (p-MLC2), an indicator for myosin ATPase activity and smooth muscle contraction[51]. Our results showed that the percentage of p-MLC2⁺ vMCs was dramatically decreased in the lesional skin of all subtypes of rosacea (Supplementary Fig. 11j, k), but the protein levels of total MLC2 were not affected (Supplementary Fig. 11l–n), revealing a deficiency of muscle contraction in vMCs in rosacea.

Next, we analyzed the changes in endothelial cells, another dominant cell type in blood vessel structures. By UMAP analysis, endothelial cells were separated into 5 subclusters (Supplementary Fig. 12a), among which subcluster 1 was significantly increased in the lesional skin of rosacea patients (Supplementary Fig. 12b, c). Further GSEA analysis showed that type I interferon signaling pathway was enriched in this subcluster, suggesting a pro-inflammatory role of endothelial cells in the pathogenesis of rosacea (Supplementary Fig. 12d).

## Fibroblasts are identified as a major determinant in rosacea

Since multiple resident cell types exhibited alterations responsible for the clinical manifestations of rosacea patients (such as increased T cell activation and differentiation for inflammation, and impaired muscle contraction of vMCs for vasodilation), we wondered which cell type plays a dominant role in orchestrating the complicated network to initiate rosacea. To this end, we performed CellChat analysis[52], to investigate the intercellular interactions among cell types in rosacea. The overall interaction number and strength were both increased in the lesional skin of all rosacea subtypes, especially in PPR (Fig. 5a and Supplementary Fig. 13a). Incoming/outgoing interaction strength results revealed that fibroblasts were the predominant cells generating outgoing signals, while immune cells like T cells, B cells and macrophages are the predominant recipient cells (Fig. 5b–d). Moreover, macrophages, endothelial cells, vMCs, keratinocytes and T cells are the primary targets for the outgoing signals of fibroblasts (Supplementary Fig. 13b–d). These results suggest a potentially critical role of fibroblasts in rosacea development.

To further determine the mechanisms by which fibroblasts are involved in the pathogenesis of rosacea, GSEA analysis was performed for each cell type using the enriched genes (compared to all other cells, Supplementary Data 10) in the lesional skin of rosacea patients. Our results showed that fibroblasts were overrepresented in categories related to the pro-inflammatory pathways (chemokine signaling pathway and cytokine-cytokine receptor interaction) and vasodilative pathway (relaxin signaling pathway) in all cell types (Fig. 5e), which was further confirmed by the expression of their signature genes, such as CCL19 and PTGDS (Fig. 5f and Supplementary Data 10). Thereinto, fibroblasts were shown to express high levels of chemokine CCL19, which was connected by ligand-receptor interactions to CCR7⁺ T cells mainly in PPR (Fig. 5g–i; Supplementary Fig. 13e). Moreover, as a vasodilation related factor synthase[53,54], PTGDS was specifically expressed in fibroblasts and significantly increased in rosacea, especially in ETR and PPR (Fig. 5j–m; Supplementary Fig. 13f, g). As a consequence, PGD₂, the product of PTGDS and a typical mediator of vasodilation[53,54], was significantly increased in the lesional skin of rosacea (Fig. 5n). The functional role of PGD₂ was further supported by the evidence showing that PTGDR, the receptor of PGD₂, was highly expressed in vMCs of the skin (Fig. 5o; Supplementary Fig. 13h). Collectively, these results suggest that the fibroblasts play the key role in cell interactions with immune and vascular mural cells in rosacea development.

Given that fibroblasts are identified as the major cell type yielding pro-inflammatory and vasodilative signals in the lesional skin, we wondered whether these cells play a functional role in the development of rosacea. To this end, we generated mice transgenic for the diphtheria toxin receptor under the control of the Col1a2 promoter (Col1a2^DTR) by mating Col1a2-CreER mice with iDTR mice. Col1a2^DTR mice allow for robust depletion of skin fibroblasts following administration of tamoxifen and diphtheria toxin (DT) (Supplementary Fig. 14a–c). We then intradermally injected cathelicidin LL37 into Col1a2^DTR and wildtype (WT) mice (Supplementary Fig. 14a), to establish rosacea-like mouse models as previously described[10,11,16,36]. Our results showed that 12 h post the last LL37 injection, WT mice displayed obvious rosacea-like dermatitis, but skin fibroblast ablation
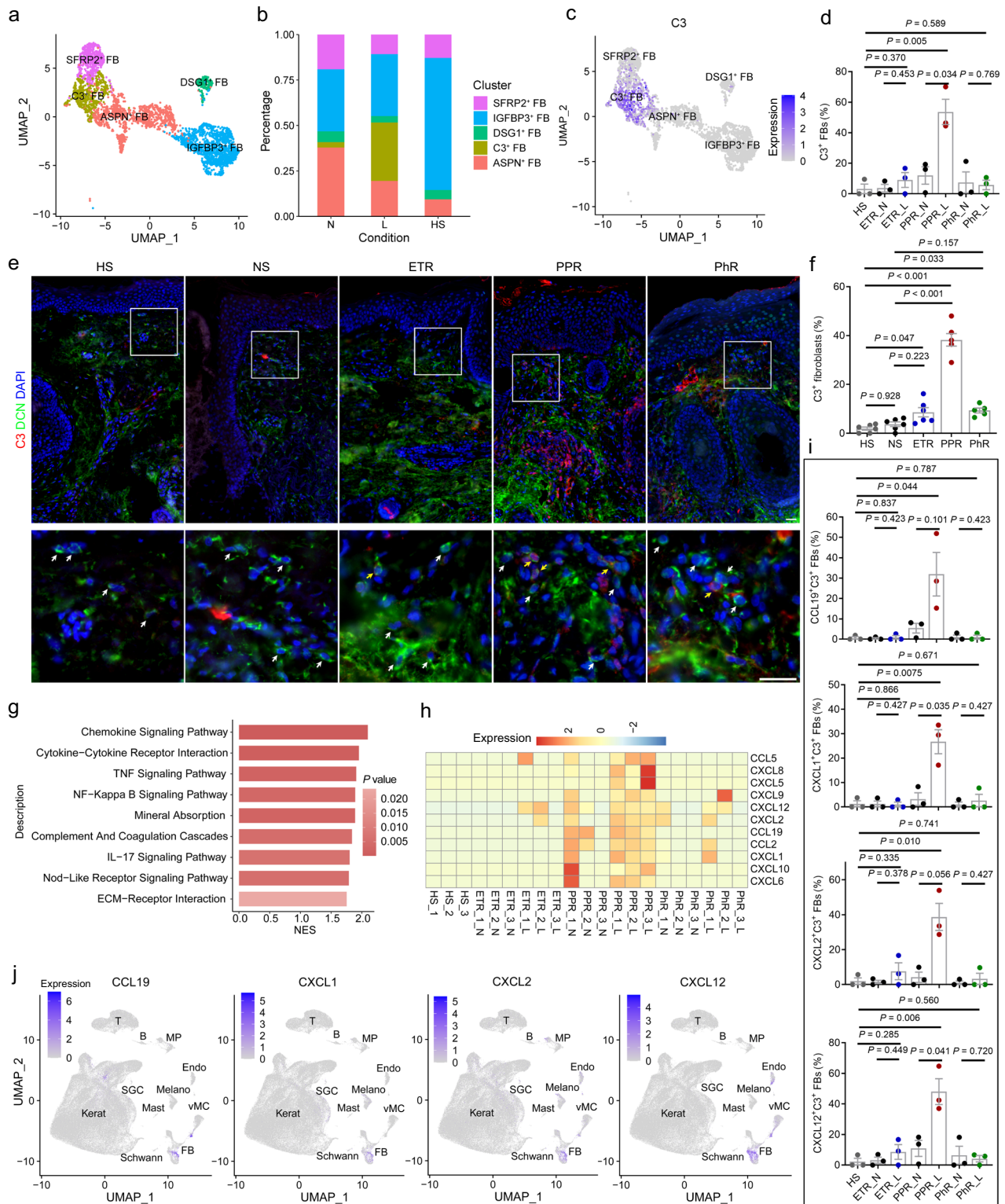
Fig. 3 | Pro-inflammatory fibroblast subpopulation is identified in rosacea.
a UMAP plots showing subclusters and sample conditions of fibroblasts. **b** Bar graph showing the percentage of subpopulations of fibroblasts. **c** Feature plot showing the expression of the C3 in fibroblasts. **d** The percentage of C3+ fibroblasts in total fibroblasts ($n = 3$ samples for each group from scRNA-seq datasets). **e** Immunohistochemistry of C3 and DCN in skin samples. Below panels are magnified images of boxed areas. White arrows indicate C3 negative fibroblasts. Yellow arrows indicate C3 positive (C3+) fibroblasts. Scale bar, 50 μm. **f** Quantification of the percentage of C3+ fibroblasts in different groups ($n = 6/6/6/6/5$ samples for HS/ NS/ETR/PPR/PhR group used in **e**). **g** The top-ranked enriched KEGG pathways in

C3+ fibroblasts revealed by GSEA. NES stands for enrichment scores. Two-sided permutation test without multiple comparison adjustments was used for GSEA analysis. **h** Heatmap showing the expression levels of multiple inflammatory factors in C3+ fibroblasts in rosacea and healthy skins. **i** The percentage of CCL19+/ CXCL1+/CXCL2+/CXCL12+ and C3+ fibroblasts in total fibroblasts ($n = 3$ samples for each group from scRNA-seq datasets). **j** Feature plots showing the expression of CCL19, CXCL1, CXCL2, CXCL12 in all cell types. Data are presented as mean ± SEM and P-values were determined by one-way ANOVA with Tukey's post hoc test (**f**), and two-tailed unpaired (L vs HS) or paired (L vs N) Student's t-test (**d**, **i**).
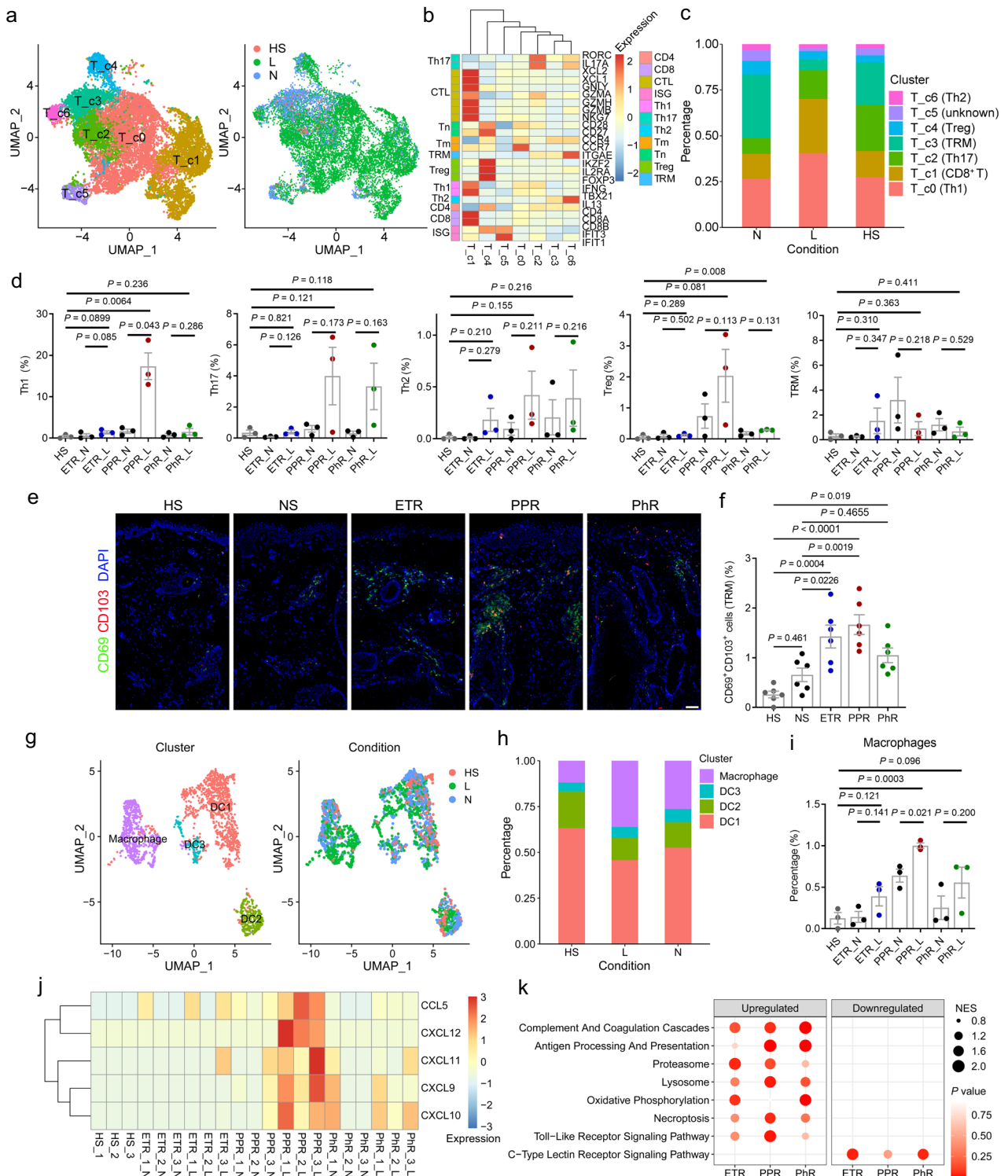
Fig. 4 | Compositional and gene expression alterations of immune cells in rosacea. a UMAP plots showing subclusters and sample conditions of T cells. **b** Heatmap showing the expression of signature genes in different subpopulations of T cells. **c** Bar graph showing the percentage of subpopulations of T cells. Th1, Type 1T helper cells; Th17, Type 17T helper cells; Th2, Type 2T helper cells; Treg, regulatory T cells; TRM, resident memory T cells. **d** The percentage of different subpopulations in total cells ($n = 3$ samples for each group from scRNA-seq datasets). **e** Immunostaining of CD69 and CD103 in skin samples. Scale bar, 50 μm. **f** Quantification of the percentage of CD69⁺CD103⁺ resident memory T cells in different groups ($n = 6/6/6/6/6$ samples for HS/NS/ETR/PPR/PhR group used in **e**). **g** UMAP plots showing subclusters and sample conditions of macrophages/DCs.

h Bar graph showing the percentage of subpopulations of macrophages/DCs. **i** The percentage of macrophages in different conditions ($n = 3$ samples for each group from scRNA-seq datasets). **j** Heatmap showing the expression levels of multiple chemokines in macrophages in rosacea and healthy skins. **k** Top-ranked enriched pathways upregulated or downregulated in macrophages in the lesional skin of rosacea. NES stands for enrichment scores. The color keys from red to blue indicate the range of *P*-value. Two-sided permutation test without multiple comparison adjustments was used for GSEA analysis. Data are presented as mean ± SEM and *P*-values were determined by one-way ANOVA with Tukey's post hoc test (**f**), and two-tailed unpaired (L vs HS) or paired (L vs N) Student's *t*-test (**d**, **i**).

Figure (panels a–o)
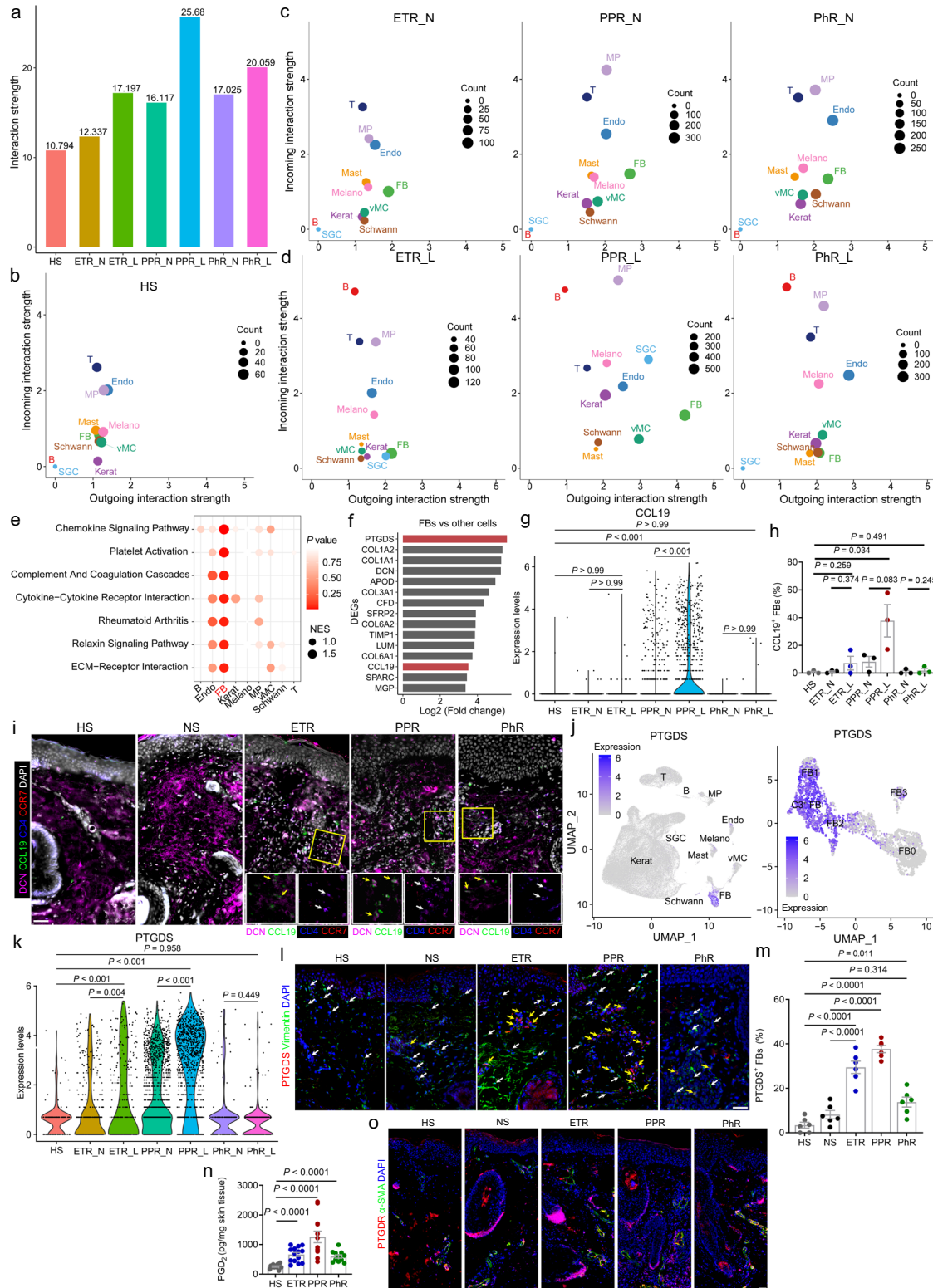
mice were unable to develop typical rosacea-like phenotypes (Fig. 6a–c). Furthermore, the inflammatory cell infiltration in the dermis and disease-characteristic inflammatory factors were also significantly improved in these mice (Fig. 6d–f).

To further verify the critical role of fibroblasts in the pathogenesis of rosacea, we focused on PTGDS, a gene specifically expressed and upregulated in fibroblasts of rosacea skin lesions (Fig. 5f, j–m). First, PTGDS was demonstrated to be also specifically expressed and

upregulated in fibroblasts of LL37-induced rosacea-like mouse model (Supplementary Fig. 15a, b). To explore the functional significance of PTGDS in rosacea development, we injected *Ptgds* and scrambled siRNAs intradermally twice at the indicated time to knockdown Ptgds in mouse skin (Supplementary Fig. 15c). Then, we verified that PTGDS and PGD$_2$ were both suppressed in LL37-injected skin after *Ptgds* siR-NAs treatment (Supplementary Fig. 15a, b and d). Our results showed that the knockdown of *Ptgds* not only dramatically improved the

Fig. 5 | Fibroblasts are identified as a major determinant for rosacea development. a The total interaction strength in rosacea and healthy skins analyzed by CellChat. **b–d** Bubble diagrams showing the incoming/outgoing interaction strength of each cell type in HS (**b**), non-lesional (**c**) and lesional (**d**) skin of rosacea. **e** KEGG categories of genes enriched in each cell type from the lesional skin of rosacea patients. Two-sided permutation test without multiple comparison adjustments was used for GSEA analysis. **f** DEGs of fibroblasts (compared to other cells) in the lesional skin of rosacea patients. **g** Violin plot showing the expression of *CCL19* in fibroblasts. **h** The percentage of CCL19$^+$ fibroblasts in total fibroblasts ($n = 3$ samples for each group from scRNA-seq datasets). **i** Multiplex immunohistochemistry of CCL19, DCN, CCR7 and CD4 in skin samples of HS ($n = 5$), NS ($n = 5$), and lesional skin of ETR ($n = 5$), PPR ($n = 5$) and PhR ($n = 5$). The presented images are representative of each group. Below panels are magnified images of boxed areas. White arrows indicate CD4$^+$CCR7$^+$

T cells. Yellow arrows indicate CCL19$^+$DCN$^+$ fibroblasts. Scale bar, 50 μm. **j** Feature plots showing the expression of PTGDS in all cells (left) and fibroblasts (right). **k** Violin plot showing the expression of *PTGDS* in fibroblasts. **l** Immunohistochemistry of PTGDS and Vimentin in skin samples. White arrows indicate Vimentin$^+$PTGDS$^-$ fibroblasts. Yellow arrows indicate Vimentin$^+$PTGDS$^+$ fibroblasts. Scale bar, 50 μm. **m** Quantification of the percentage of PTGDS$^+$ fibroblasts ($n = 6/6/6/6/6$ samples for HS/NS/ETR/PPR/PhR group used in **l**). **n** Levels of PGD$_2$ in skin samples, detected by ELISA ($n = 11/14/12/11$ samples for HS/ ETR/PPR/PhR group). **o** Immunohistochemistry of PTGDR and α-SMA in skin samples of HS, normal skin of rosacea patients (NS), and lesional skin of ETR, PPR and PhR. Scale bar, 50 μm. Data are presented as mean ± SEM and *P*-values were determined by one-way ANOVA with Tukey's post hoc test (**g**, **k**, **m**), and two-tailed unpaired (L vs HS) or paired (L vs N) Student's *t*-test (**h**, **n**).

rosacea-like features (Fig. 6g–i), but also decreased the dermal infiltrating cells and inflammatory factors in mice (Fig. 6j, k; Supplementary Fig. 15e). Consistently, CCL19$^+$ fibroblasts and CCR7$^+$ T cells were abrogated after *Ptgds* siRNAs administration in LL37-injected skin (Supplementary Fig. 15f–i). Moreover, by immunohistochemistry (IHC) of CD31, we demonstrated that *Ptgds* knockdown improved the abnormal dilation of blood vessels (Fig. 6l, m), which was further supported by immunostaining of p-MLC2 (Supplementary Fig. 15j, k).

Taken together, these findings demonstrate that fibroblasts act as a major determinant in the pathogenesis of rosacea.

Discussion

Although rosacea is considered to be involved in the dysregulation of cutaneous nervous, immune and vascular systems, the precise cell composition and their molecular alterations and functions in cutaneous lesions in this disorder remain unclear.

Here we have presented what, to the best of our knowledge, is currently the only comprehensive single-cell transcriptomic analysis of all cell types within skin lesions from patients with rosacea compared with healthy individuals. Our scRNA-seq atlas of rosacea and healthy skin contains 11 broad cell types. By high-resolution subclustering, functional analysis and experimental validation, we identified multiple subpopulations associated with rosacea in different cell types.

Skin barrier is impaired in rosacea skin lesions characterized by decreased expression of multiple barrier genes, especially CLDNs, which might be responsible for the exacerbation of inflammation[7,8,55]. Our scRNA-seq data here identify a subpopulation of keratinocytes increased in the lesional skin of all rosacea subtypes, which is featured by barrier function damage, including declined tight junction, adherens junction and cell adhesion molecules. Furthermore, based on scRNA-seq data analysis and functional experimentation, we demonstrate that the upregulated type II IFN (IFNγ) signaling might contribute to the impaired skin barrier, especially for the downregulated CLDNs in keratinocytes in rosacea. Our previous bulk RNA sequencing study on rosacea whole and epidermal skin also showed that aberrant activation of epidermal IFN/STAT1 is shared across ETR, PPR and PHR Subtypes[34]. To be mentioned, although type I IFNs are not detected, our results here show that type I IFN signaling is among the top upregulated pathways in rosacea. We speculate that type I and II IFN signaling pathways share very similar downstream genes; although these shared genes are upregulated in response to type II rather than type I IFN, they were also included in the gene set of type I IFN signaling pathway when GSEA was performed. Collectively, these findings might provide an upstream explanation for the impaired skin barrier in rosacea.

However, a recent study has shown that the expression of type I IFNs, including *IFNA2* and *IFNB1*, is significantly increased in plasmacytoid dendritic cells of the lesional skin from rosacea patients during acute flares, but not changed during stable disease. They further revealed dysbiotic commensal bacteria are

responsible for the production of type I IFNs. In addition, blockade of type I IFN signaling could partially improve the rosacea-like phenotypes in the same rosacea mouse model used in our study[56], but the treatment appeared to be less effective than blockade of IFNγ. Therefore, it is assumed that type I IFNs might only be produced in skin lesions with dysbiotic commensal bacteria, which may be an aggravating factor rather than an initiating factor for rosacea development. Moreover, the products of microbiome can be recognized by keratinocytes and cells of the innate immune system, then activate Toll-like receptors; further activation of inflammatory receptors can aggravate the impaired skin barrier, which may result in more inflammation[6,56–58]. Here, our results show that antigen processing and presentation and Toll-like receptor signaling pathways are upregulated in multiple cell types, including keratinocytes, macrophages and Schwann cells, suggesting a possible link between abnormal microbiome and inflammation. However, further study is needed to clarify the direct role of microbiome in rosacea.

Increasing evidence has demonstrated that rosacea is a kind of neurogenic skin inflammation[5,6,38,39]. Our recent study also identified multiple genetic variants associated with neurogenic inflammation, which can promote rosacea development by modulating the production of neuropeptides in peripheral neurons[36]. However, the cellular and molecular changes in the local cutaneous neural system remain largely unclear. In the present study, although neuron cells are not found in our scRNA-seq datasets, possibly due to the fact that the cell bodies of neurons are not located in skin, we uncover a cluster of Schwann cells, a type of glial cell that surrounds the neurons and plays a critical role in the maintenance and function of peripheral nerves[59]. Previous studies have revealed neuroinflammatory roles of Schwann cells in multiple inflammatory neuropathies, such as Chronic inflammatory demyelinating polyneuropathy (CIDP) and Guillain-Barre syndrome (GBS)[60–63]. Consistently, we here identify a previously undefined subpopulation of Schwann cells unique to rosacea skin lesions, which is characterized by the upregulation of multiple pro-inflammatory pathways. However, further study is needed to illustrate the precise mechanisms by which Schwann cells participate in the pathogenesis of rosacea, and it will be very interesting to figure out the landscape of peripheral neural signatures and their interaction with other cells in the skin lesions of rosacea possibly by burgeoning technologies, such as single-cell spatial proteomics.

Rosacea is well established as a chronic inflammatory skin disorder, and the dominating infiltrating cells are T cells, macrophages and mast cells[9]. Therein, Th1/Th17 polarization and macrophage infiltration are considered as an undervalued hallmark across all subtypes of rosacea[64]; mast cell activation has also been suggested to be involved in skin inflammation of rosacea[65,66]. We here elucidate the landscape of cutaneous immune cells at single-cell level in the lesional skin of different subtypes of rosacea. In agreement with previous studies, T cells are the major infiltrating cells, and Th1/Th17 cell
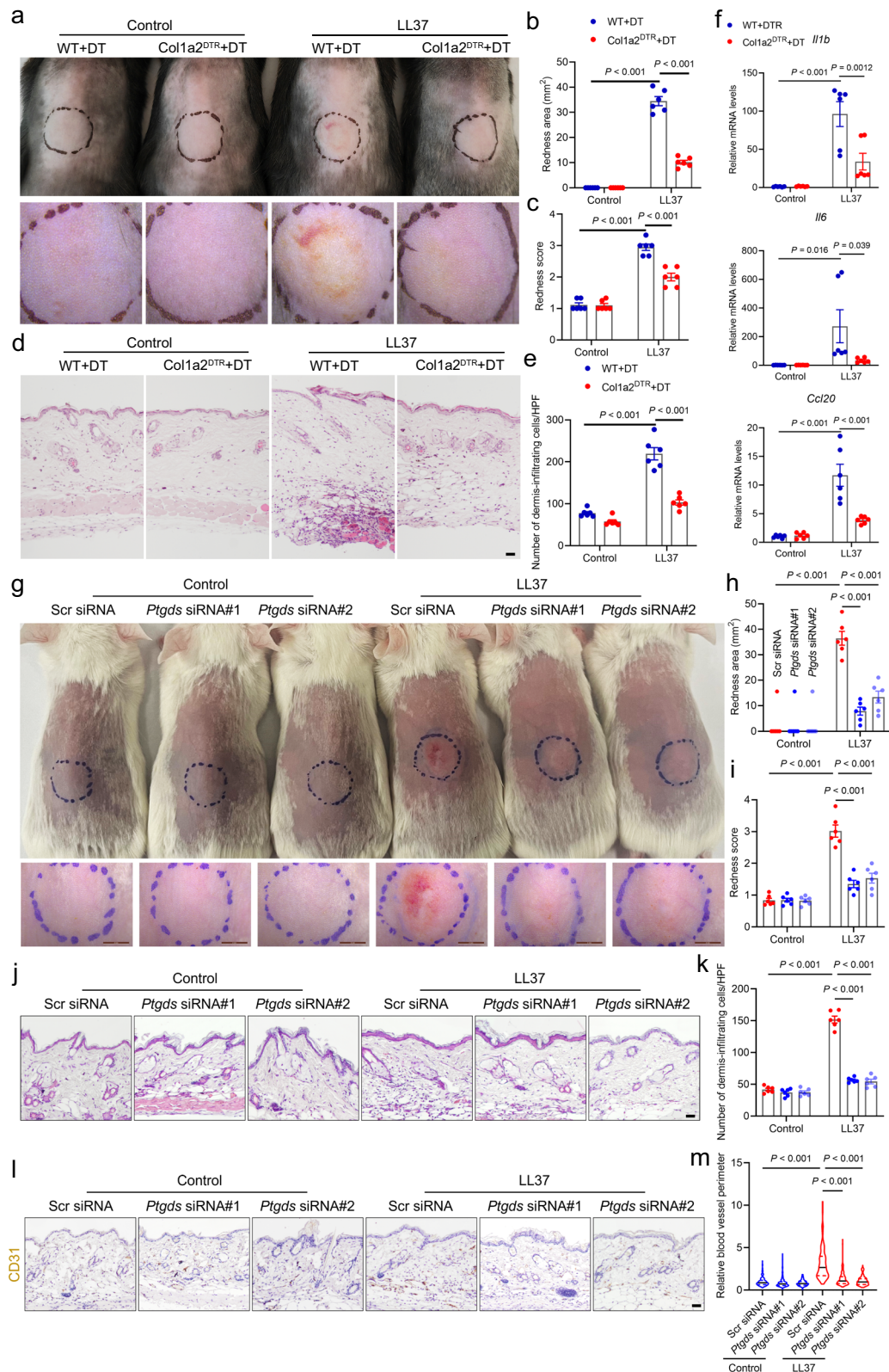
differentiation is significantly increased across all rosacea subtypes, especially in PPR. Unexpectedly, we find that resident memory T cells are expanded in rosacea, which might provide a cellular explanation for the easy recurrence of this disorder. Macrophages, considered as the master regulators of inflammation[67], are increased in all subtypes of rosacea, and express high levels of multiple T cell-recruiting chemokines, such as CCL5, CXCL9, CXCL10, CXCL11. Moreover, B cell infiltration is shown to be increased in PPR skin lesions, but the potential roles need further study to clarify.

In addition to inflammation, vascular dysfunction, including validation and angiogenesis, is another hallmark of rosacea[6,9,11,38]. We here demonstrate that the percentage of vascular endothelial cells is

Fig. 6 | Fibroblasts are essential for rosacea development in mice. a The back skins of WT and Col1a2[DTR] mice intradermally injected with LL37 or control vehicle. Images were taken 12 h after the last LL37 injection. Below panels are magnified images of black circled areas. **b, c** The severity of the rosacea-like phenotypes after the first LL37 injection for 48 h, was evaluated with the redness area (**b**) and score (**c**) ($n = 6$ for each group). **d** HE staining of lesional skin sections from WT and Col1a2[DTR] mice treated with LL37 or control vehicle. Scale bar, 50 μm. **e** Dermal infiltrating cells were quantified ($n = 6$ for each group). **f** The relative mRNA levels of *Il1β*, *Il6* and *Ccl20* in mice lesional skins ($n = 6$ mice for each group). **g** The back skins of Scr or *Ptgds* siRNAs-treated WT mice intradermally injected with LL37 or control vehicle. Images were taken 12 h after the last LL37 injection. Below panels are magnified images of blue-circled areas. **h, i** The severity of the rosacea-like phenotypes 48 h after the first LL37 injection, was evaluated with the redness area (**h**) and score (**i**) ($n = 6$ for each group). **j** HE staining of lesional skin sections. Scale bar, 50 μm. **k** Dermal infiltrating cells were quantified ($n = 6$ for each group). **l** Immunohistochemistry of CD31 on skin sections. Scale bar, 50 μm. **m** Quantification of relative blood vessel perimeter in the corresponding groups displayed with violin plot. $n = 117$–181 blood vessels from five independent mice for each group. All results are representative of at least three independent experiments. Data are presented as mean ± SEM, and *P*-values were determined by one-way ANOVA with Tukey's post hoc test.

increased in skin lesions of rosacea, especially in PPR and PhR, which further supports our previous findings showing that angiogenesis is augmented and might be necessary for rosacea development[68]. Besides endothelial cells, blood vessels contain a cluster of vascular mural cells (including vSMCs and pericytes) that make up most of the vessel walls, which are essential for vascular contraction and relaxation[69]. Here, though changes in muscle contraction are not identified in our scRNA-seq datasets, we show that the phosphorylation levels of MLC2 are greatly decreased in vMCs in all subtypes of rosacea, even in the non-lesional skin, which might be the direct cause of abnormal validation of blood vessels in rosacea. We speculate that the muscle contraction of vMCs is likely determined by post-transcriptional regulation, such as protein phosphorylation, in rosacea.

Various studies have roughly revealed the cellular and molecular alterations through global gene analysis and immunohistochemistry[7,12–16], and our present study illustrates the changes of different cell types in rosacea skin lesions at single-cell level, but the intercellular communications among cell types remain largely unknown. In the present study, via cell-cell communication analysis, we identify fibroblasts as the leading cell type producing outgoing signals, and T cells, macrophages, vMCs, keratinocytes and endothelial cells are the main target cells for these outgoing signals, suggesting a pivotal role for fibroblasts in the pathogenesis of rosacea. Previous scRNA-seq studies showed that fibroblasts could contribute to the amplification of inflammatory responses via transition to a pro-inflammatory state and production of multiple chemokines, both in psoriasis and atopic dermatitis. For instance, these fibroblasts could produce CCL19, connected by ligand-receptor interactions to CCR7+ dendritic cells in the lesional skin[21,70]. Consistently, we here demonstrate that in rosacea, fibroblasts are reprogrammed into a pro-inflammatory state, featured by expressing high levels of disease-characteristic chemokines, like CCL19, CXCL1, CXCL2 and CXCL12. Specifically, these reprogrammed fibroblasts generate abundant CCL19, which recruits CCR7+ T cells, the dominant infiltrating cells, by ligand-receptor interactions in the lesional skin of rosacea. In addition to the pro-inflammatory outgoing signals, fibroblasts are also identified as the leading cell type producing outgoing signals related to vascular relaxation. Among these vascular relaxation-associated signals, PTGDS, an enzyme that catalyzes the conversion of prostaglandin H2 (PGH$_2$) to prostaglandin D2 (PGD$_2$), is specifically expressed and remarkably upregulated in fibroblasts of the lesional skin of all rosacea subtypes. As a consequence, PGD$_2$, a classical mediator of vasodilation[53,54], is significantly increased in the skin lesions. As expected, PTGDR, the receptor of PGD$_2$, is found to be specifically and highly expressed in the cutaneous vMCs, suggesting that fibroblasts contribute to abnormal vasodilation via PGD$_2$-PTGDR axis in rosacea. We conclude that fibroblasts are the leading cell type producing pro-inflammatory and vasodilative signals in the pathogenesis of rosacea.

Our study is not without limitations. First, due to the small sample size used in this study, further investigations are needed to elucidate some assumptions directly drawn from our scRNA-seq datasets.

Second, considering that only female human samples are used, we cannot rule out that all of the present findings apply to the male, and further experiments will be needed to clarify this issue. Third, given that the healthy skin samples were dominated by keratinocytes, this caveat should be kept in mind regarding the findings for cellular proportion, especially for the cell type in which less than 10 cells are collected.

In summary, the present study illustrates the cellular and molecular landscape of skin-resident cell populations, and determines fibroblasts as the pivotal determinant in the development of rosacea, emphasizing the role of mesenchymal subpopulations in the treatment of this disorder.

Methods

Human skin samples

This study was approved by the ethical committee of the Xiangya Hospital of Central South University (No. 201404361). All skin biopsies were collected from the central facial skin of female healthy volunteers, and lesional skin of the central face and corresponding normal skin surrounding the auricle from female patients with ETR, PPR and PhR (aged 20–45 years) from the Dermatology of Xiangya Hospital, Central South University. Patients were diagnosed with rosacea by clinical and pathologic examination. The use of human samples was reviewed and approved in advance by the Ethical Committee of the Xiangya Hospital, Central South University, and written informed consent was obtained from all participants, and the participants received no compensation for their participation. All experiments were conducted according to the principles set out in the WMA Declaration of Helsinki and the Department of Health and Human Services Belmont Report.

Preparation of single-cell suspension of human skin biopsies

The whole tissue processing and the single-cell preparation process were completed within 3 h after the collection of surgical skin biopsies. After removal of subcutaneous fat, skin samples were placed in a dish with 5 ml of dispase solution by dermis side down and incubated at 37 °C with shaking (80 rpm) for 60 min. Epidermis was carefully isolated from the dermis with forceps. The separated epidermis was placed in 5 ml of trypsin at 37 °C for 10 min, and the separated dermis was digested with 10 ml of collagenase V for 45 min, then neutralized with 5% FBS in PBS. The single-cell suspension was acquired by repeatedly aspirating and dispensing the solution with a 1-ml pipette and then filtered through 70 μm and 40 μm strainers. The dead cells were removed with Dead Cell Removal Kit (Miltenyi Biotec). For each sample, all of the epidermis and dermis cells were pooled together for the next step of single-cell analysis.

ScRNA-seq

scRNA-seq primarily involves GEM (gel bead-in-emulsion) generation, barcoding, cDNA amplification, library construction and sequencing. These steps were performed in accordance with the user's instructions of Chromium Single Cell 3′ Reagent Kits v3.1 (10× Genomics). Libraries were sequenced by an Illumina NovaSeq6000 System. Approximately

10,000 cells (targeting 5000–12,000) per sample were subjected to single-cell RNA sequencing.

Processing of scRNA-seq data

The raw reads data were mapped to the hg38 human genome to perform quality control and the read counting of Ensemble genes using Cell Ranger (v6.0.2) (http://10xgenomics.com) with default parameters. Seurat (v4.3.0) R package was used to exclude cells with fewer than 200 genes or more than 6000 genes detected and more than 20% mitochondrial reads for downstream analysis[71].

After quality control, 131,243 cells remained and were used for downstream bioinformatic analysis. The "SCTransform" function with default parameters was used to normalize and scale the feature expression measurements for each cell by the total expression. The initial cell clustering was performed by "FindClusters" function by their first 20 PCs with Louvain algorithm at a resolution of 0.6. Non-linear dimensional reduction was performed by "RunUMAP" function and visualized by Uniform Manifold Approximation and Projection (UMAP). Markers genes of each cell cluster were determined by "FindAllMarkers" function with Wilcoxon rank-sum test. Only those with |'avg_logFC'| ≥0.25 and 'p_val_adj' ≤0.05 were considered as marker genes.

For subclustering analysis of each major cell type, cells were extracted separately and clustered by their first 20 PCs and appropriate resolution. Markers genes of each subcluster were identified by "FindAllMarkers" function with the default parameters. "DoHeatmap" function was used to show the top 20 markers gene in heatmap.

Profiling differentially expressed genes within each condition

To identify differentially expressed genes between lesional and non-lesional skin, we applied the "FindMarkers" function from Seurat with the following parameters: min.pct >0.25 and thresh.use = 0.25. The adjusted p-value of each differentially expressed gene was calculated by non-parametric two-sided Wilcoxon rank-sum test and only those with |'avg_logFC'| >0.25 and 'p_val_adj' < 0.05 were considered to be differentially expressed genes. The gene expression levels shown in the various charts in the manuscript were plotted using packages in R.

Function enrichment analysis

Gene Set Enrichment Analysis (GSEA) of GO and KEGG was performed by clusterProfiler R package (v4.5.1.902) and visualized with ggplot2 R package (v3.4.1)[72]. Representative terms that were significantly enriched in at least one of the three rosacea subtypes, or top-ranked GO terms and KEGG pathways from MsigDB, were displayed.

Cell-cell communication analysis

To assess cell-cell communications among different cell types, we used CellChat (v1.1.3) to infer the intercellular communication network from single-cell RNA-seq data. Only cell types with more than 10 cells were considered in this analysis. The "trimean" method is used for calculating the average gene expression in "computeCommunProb" function. Pairwise comparison and visualization are performed by CellChat build-in function, only interactions with P-value lower than 0.05 are considered to be significant.

Mouse model of rosacea and treatments

BALB/c and C57BL/6J wildtype mice were purchased from Slark Company. The dorsal skin of the mice, aged 7 to 8 weeks, was shaved 1 day before the beginning of treatments. For the mouse model of rosacea, intradermal injection of 40 µl LL37 (320 µM, Sangon Biotech) was applied on the dorsal skin twice a day for 2 days, as previously described[10,16,36].

For IFNγ blocking, neutralizing IFNγ antibodies (10 µg/mice; eBioscience) were subcutaneously injected daily before and during the LL37 injection for a total of 3 days in BALB/c wildtype mice aged 8 weeks. The first treatment dose began one day prior to the intradermal injection of LL37. An identical dose of IgG was administered to the control mouse. To deplete local skin fibroblasts, *Col1a2*-CreER mice with C57BL/6J background (Jackson Laboratory, Strain #029567) were mated with iDTR mice with C57BL/6J background (Jackson Laboratory, Strain #007900). *Col1a2*-CreER/iDTR double positive (Col1a2^DTR) and WT mice were treated with tamoxifen (150 mg/kg, Sigma) daily for continuous five days at 5 weeks of age by intraperitoneal injection. 1 week after tamoxifen treatment, mice were intradermally injected with diphtheria toxin (DT, 100 ng per mice, sigma) once daily for 3 days. The identical location that had received DT was intradermally injected with LL37 one week later. For siRNA-mediated Ptgds knockdown in mice, *Ptgds* or scrambled siRNAs (20 µL of 20 µM, purchased from the GenePharma company) were intradermally injected at the indicated site of dorsal skin at indicated time in BALB/c wildtype mice aged 7 weeks. The oligo sequences of siRNAs used in this study are provided in Supplementary Data 11.

The dorsal skin lesions were observed using a stereoscope and harvested for subsequent experiments (including histological analysis, immunohistochemistry, immunofluorescence, ELISA, RT-qPCR, etc.) 48 h after the first LL37 injection in all mice studies, and were scored for redness and area as previously described[36]. All mouse experiments were repeated three times, and 5–6 mice were included in each group in each experiment. All mouse experiments were performed on both female and male mice, and there is no sex difference in the above mouse experiments, and the results of female mice were presented in this study. Mice were randomly assigned to different groups and sex-matched in each experiment. All mice used in the presented study were housed in specific pathogen-free conditions with a regular 12 h light/12 dark cycle at -20–25 °C and 45–55% humidity and were fed standard rodent chow and tap water. Animal welfare was monitored, euthanasia was conducted according to the guidelines, and the ethical committee of the Xiangya Hospital of Central South University approved all animal procedures.

Histological analysis

The dorsal skin tissues of the mice were fixed and embedded in paraffin. Paraffin sections were deparaffinized and stained with H&E solution. To examine histological changes, we count the number of infiltrating cells in the dermis. Five randomly selected locations in each section were used to calculate the number of infiltrating cells in the dermis.

Immunohistochemistry

Immunohistochemistry for mouse skin sections (5 µm) was conducted as previously described[36]. To assess the vasodilation of cutaneous blood vessels, the perimeter of CD31-positive vessels was measured by ImageJ. Double immunohistochemistry of human or mouse skin sections was performed using Opal™ 7-Color Manual IHC Kit according to the manufacturer's protocols. Briefly, slides were deparaffinization and rehydration. Before epitope retrieval, slides were fixed in 10% neutral buffered formalin for 30 min. Slides were cooled down at room temperature and washed twice with TBST (TBS buffer containing 0.05% TritonX-100). Slides were covered with blocking buffer for 10 min, followed by incubation with primary antibody overnight at 4 °C. Slides were washed and incubated with Polymer HRP secondary antibody for 10 min at room temperature. Slides were then washed and incubated with appropriate Opal Fluorophore to amplify the fluorescence signal. Multiplex staining was performed by stripping the previous antibody in AR buffer before blocking and probing with the next primary antibody. Following similar steps from the first round of staining, slides were developed to stain for other targets. Slides were counter-stained with DAPI for 5 min, and coverslipped with mounting medium. For CD31 staining, DAB staining kit (PV-9001, ZSGB-BIO) was used according to the manufacturer's instructions. The fluorescence

intensity was assessed with ImageJ. The following primary antibodies were used: Rabbit anti-CD31 (1:100, 77699, Cell Signaling), Mouse anti-KRT14 (1:1000, ab7800, abcam), Rabbit anti-KRT14 (1:2000, ab181595, abcam), Rabbit anti-CD74 (1:500, 77274, Cell signaling), Rabbit anti-CD74 (1:2000, ab289885, abcam), Rabbit anti-CLDN4 (1:2000, ab210796, abcam), Rabbit anti-complement C3 (1:400, HPA003563, Atlas Antibodies), Rabbit anti-DCN (1:2000, ab277636, abcam), Rabbit anti-MBP (1:1500, 78896, Cell signaling), Rabbit anti-CD69 (1:500, ab233396, abcam), Rabbit anti-CD103 (1:2000, ab224202, abcam), Rabbit anti-p-MLC2 (1:200, 3671, Cell signaling), Mouse anti-α-SMA (1:5000, ab7817, abcam), Mouse anti-CCL19 (1:100, MAB361, R&D systems), Mouse anti-CD4 (1:200, 14-2444-80, Thermo), Mouse anti-CCR7 (1:100, MAB197, R&D systems), Rabbit anti-PTGDS (1:200, HPA004938, Atlas Antibodies), Rabbit anti-Vimentin (1:400, 5741, Cell signaling), Rabbit anti-PTGDR (1:200, HPA049668, Atlas Antibodies). Rabbit anti-p-STAT1 (1:1000, 9167, Cell signaling), Rabbit anti-IRF1 (1:200, 8478, Cell signaling).

Immunofluorescence

Skin lesions from human or mice were obtained and embedded in OCT. The sections were fixed with 4% paraformaldehyde and blocked with 5% donkey serum in PBS for 1 h at room temperature. The sections were incubated with primary antibodies overnight (4 °C) and then were incubated with secondary antibodies for 1 h (room temperature). DAPI staining was used to indicate the cell nucleus. The quantification of fluorescence intensity was conducted with ImageJ, as previously described[36]. The following primary antibodies were used: Goat anti-PDGFRA antibody (1:100, AF1062, R&D systems), Rabbit anti-PTGDS antibody (1:200, 10004344, Cayman), Rabbit anti-PDGFRA (1:500, ab203491, abcam), Goat anti-CCL19 (1:100, AF880, R&D systems), Rabbit anti-CD4 (1:500, ab183685, abcam), Rat anti-CCR7 (1:100, MAB3477, R&D systems), Rat anti-IFNγ (1:100, 14-7311-81, Thermo), Rabbit anti-MBP (1:1500, 78896, Cell signaling), Sheep anti-CD74 (1:100, AF7478, R&D systems), Rat anti-F4/80 (1:100, 14-4801-81, Thermo), Goat anti-CXCL10 antibody (1:100, AF466, R&D systems), Rabbit anti-MLC2 (1:400, 15354-1-AP, Proteintech), Mouse anti-α-SMA (1:5000, ab7817, abcam).

Measurement of TEWL

TEWL was assessed with Tewameter® TM 300 (Courage + Khazaka Electronic, Germany). An average value of three repeated measurements was used for each mouse, and all measurements were conducted by the same investigator.

Enzyme-linked immunosorbent assay (ELISA)

The concentration of Prostaglandin D2 (PGD$_2$) in skin lesions from rosacea patients, healthy individuals and mice was quantified using a PGD$_2$ ELISA kit (512031-96stripwells, Cayman) according to the manufacturer's protocol.

Cell culture and treatment

Primary human keratinocytes were isolated from human foreskin (aged 2–5) and cultured in CnT-07 (CELLnTEC, USA). For IFNγ treatment, at a confluency of 40%, cells were treated with IFNγ (500 IU/ml) for 48 h, then the cells were subjected to subsequent analysis.

RT-qPCR

Total RNA from skin lesion and keratinocytes was extracted by TRIzol reagent (Thermo) and then reverse-transcribed to cDNA using the PrimeScript RT Reagent Kit (Thermo). qPCR was performed using 2x Taq Pro Universal SYBR qPCR Master Mix (Vazyme). The relative mRNA expression levels were calculated based on the $2^{-\Delta\Delta CT}$ method. The sequences of the primers used in this study are provided in Supplementary Data 11.

Statistical analysis

Statistical analyses were performed using GraphPad Prism (version 8). All data are presented as the mean ± SEM. We determined the data for normal distribution and similar variance between groups. The differences between 2 groups were compared by 2-tailed unpaired or paired Student's t-test. For comparisons of more than 2 groups, one-way ANOVA with Tukey's post hoc test or two-way ANOVA with a post hoc Holm–Sidak's multiple comparisons test was performed. Two-sided permutation test without multiple comparison adjustments was used for GSEA analysis. When the data were not normally distributed or exhibited unequal variances between groups, we performed statistical analysis with two-tailed Mann–Whitney U test. No statistical method was employed to predetermine the sample size. Mice in this study were randomly allocated to different groups.

Reporting summary

Further information on research design is available in the Nature Portfolio Reporting Summary linked to this article.

Data availability

All data needed to evaluate the conclusions in this study are provided in the manuscript and/or the Supplementary Materials. The scRNA-seq datasets are available from the genome sequence archive under accession number HRA006167 (http://bigd.big.ac.cn/gsa-human/). Bulk RNA-seq datasets for the skin lesions of rosacea patients used in this study were obtained from the genome sequence archive under accession number HRA000379 (http://bigd.big.ac.cn/gsa-human/). All relevant approvals were obtained from China's Ministry of Science and Technology related to the export of genetic information and materials relevant to this work. Any other details supporting the findings of the present study are available from the corresponding author upon reasonable request. Source data are provided with this paper.

References

1. van Zuuren, E. J. Rosacea. *N. Engl. J. Med.* **377**, 1754–1764 (2017).
2. Gether, L., Overgaard, L. K., Egeberg, A. & Thyssen, J. P. Incidence and prevalence of rosacea: a systematic review and meta-analysis. *Br. J. Dermatol.* **179**, 282–289 (2018).
3. Li, J. et al. Epidemiological features of rosacea in Changsha, China: a population-based, cross-sectional study. *J. Dermatol.* **47**, 497–502 (2020).
4. Wilkin, J. et al. Standard classification of rosacea: report of the National Rosacea Society Expert Committee on the classification and staging of rosacea. *J. Am. Acad. Dermatol.* **46**, 584–587 (2002).
5. Gallo, R. L. et al. Standard classification and pathophysiology of rosacea: the 2017 update by the National Rosacea Society Expert Committee. *J. Am. Acad. Dermatol.* **78**, 148–155 (2018).
6. Buddenkotte, J. & Steinhoff, M. Recent advances in understanding and managing rosacea. *F1000Res* **7**, F1000 Faculty Rev-1885 (2018).
7. Medgyesi, B. et al. Rosacea is characterized by a profoundly diminished skin barrier. *J. Invest. Dermatol.* **140**, 1938–1950.e1935 (2020).
8. Deng, Z. et al. Claudin reduction may relate to an impaired skin barrier in rosacea. *J. Dermatol.* **46**, 314–321 (2019).
9. Steinhoff, M. et al. Clinical, cellular, and molecular aspects in the pathophysiology of rosacea. *J. Investig. Dermatol. Symp. Proc.* **15**, 2–11 (2011).
10. Deng, Z. et al. A positive feedback loop between mTORC1 and cathelicidin promotes skin inflammation in rosacea. *EMBO Mol. Med.* **13**, e13560 (2021).
11. Liu, T. et al. Aberrant amino acid metabolism promotes neurovascular reactivity in rosacea. *JCI Insight* **7**, e161870 (2022).

12. Zhang, H. et al. Murine models of rosacea: a review. *J. Cosmet. Dermatol.* **21**, 905–909 (2022).

13. Ahn, C. S. & Huang, W. W. Rosacea pathogenesis. *Dermatol. Clin.* **36**, 81–86 (2018).

14. Shih, Y. H., Xu, J., Kumar, A., Li, R. & Chang, A. L. S. Alterations of immune and keratinization gene expression in papulopustular rosacea by whole transcriptome analysis. *J. Invest. Dermatol.* **140**, 1100–1103.e1104 (2020).

15. Woo, Y. R., Lim, J. H., Cho, D. H. & Park, H. J. Rosacea: molecular mechanisms and management of a chronic cutaneous inflammatory condition. *Int. J. Mol. Sci.* **17**, 1562 (2016).

16. Yamasaki, K. et al. Increased serine protease activity and cathelicidin promotes skin inflammation in rosacea. *Nat. Med.* **13**, 975–980 (2007).

17. Papalexi, E. & Satija, R. Single-cell RNA sequencing to explore immune cell heterogeneity. *Nat. Rev. Immunol.* **18**, 35–45 (2018).

18. Potter, S. S. Single-cell RNA sequencing for the study of development, physiology and disease. *Nat. Rev. Nephrol.* **14**, 479–492 (2018).

19. Mereu, E. et al. Benchmarking single-cell RNA-sequencing protocols for cell atlas projects. *Nat. Biotechnol.* **38**, 747–755 (2020).

20. Kim, D., Chung, K. B. & Kim, T. G. Application of single-cell RNA sequencing on human skin: technical evolution and challenges. *J. Dermatol. Sci.* **99**, 74–81 (2020).

21. He, H. et al. Single-cell transcriptome analysis of human skin identifies novel fibroblast subpopulation and enrichment of immune subsets in atopic dermatitis. *J. Allergy Clin. Immunol.* **145**, 1615–1628 (2020).

22. Liu, X. et al. Single-cell RNA-sequencing reveals lineage-specific regulatory changes of fibroblasts and vascular endothelial cells in keloids. *J. Invest. Dermatol.* **142**, 124–135.e111 (2022).

23. Hughes, T. K. et al. Second-strand synthesis-based massively parallel scRNA-Seq reveals cellular states and molecular features of human inflammatory skin pathologies. *Immunity* **53**, 878–894.e877 (2020).

24. Sole-Boldo, L. et al. Single-cell transcriptomes of the human skin reveal age-related loss of fibroblast priming. *Commun. Biol.* **3**, 188 (2020).

25. Zheng, M. et al. Single-cell sequencing shows cellular heterogeneity of cutaneous lesions in lupus erythematosus. *Nat. Commun.* **13**, 7489 (2022).

26. Jiang, Y. et al. Cytokinocytes: the diverse contribution of keratinocytes to immune responses in skin. *JCI Insight* **5**, e142067 (2020).

27. Kabashima, K., Honda, T., Ginhoux, F. & Egawa, G. The immunological anatomy of the skin. *Nat. Rev. Immunol.* **19**, 19–30 (2019).

28. Ter Horst, B., Chouhan, G., Moiemen, N. S. & Grover, L. M. Advances in keratinocyte delivery in burn wound care. *Adv. Drug Deliv. Rev.* **123**, 18–32 (2018).

29. Kim, Y. M. & Shin, E. C. Type I and III interferon responses in SARS-CoV-2 infection. *Exp. Mol. Med.* **53**, 750–760 (2021).

30. Kanoh, H. et al. IFN-gamma reduces epidermal barrier function by affecting fatty acid composition of ceramide in a mouse atopic dermatitis model. *J. Immunol. Res.* **2019**, 3030268 (2019).

31. Mizutani, Y., Takagi, N., Nagata, H. & Inoue, S. Interferon-gamma downregulates tight junction function, which is rescued by interleukin-17A. *Exp. Dermatol.* **30**, 1754–1763 (2021).

32. Hile, G. A., Gudjonsson, J. E. & Kahlenberg, J. M. The influence of interferon on healthy and diseased skin. *Cytokine* **132**, 154605 (2020).

33. Srivastava, A. et al. Cross-talk between IFN-gamma and TWEAK through miR-149 amplifies skin inflammation in psoriasis. *J. Allergy Clin. Immunol.* **147**, 2225–2235 (2021).

34. Deng, Z. et al. Keratinocyte-immune cell crosstalk in a STAT1-mediated pathway: novel insights into rosacea pathogenesis. *Front. Immunol.* **12**, 674871 (2021).

35. Wei, K., Nguyen, H. N. & Brenner, M. B. Fibroblast pathology in inflammatory diseases. *J. Clin. Invest.* **131**, e149538 (2021).

36. Deng, Z. et al. Whole genome sequencing identifies genetic variants associated with neurogenic inflammation in rosacea. *Nat. Commun.* **14**, 3958 (2023).

37. Zhu, Y., Duan, S., Wang, M., Deng, Z. & Li, J. Neuroimmune interaction: a widespread mutual regulation and the weapons for barrier organs. *Front. Cell Dev. Biol.* **10**, 906755 (2022).

38. Schwab, V. D. et al. Neurovascular and neuroimmune aspects in the pathophysiology of rosacea. *J. Investig. Dermatol. Symp. Proc.* **15**, 53–62 (2011).

39. Aubdool, A. A. & Brain, S. D. Neurovascular aspects of skin neurogenic inflammation. *J. Investig. Dermatol. Symp. Proc.* **15**, 33–39 (2011).

40. Wang, S. et al. S100A8/A9 in Inflammation. *Front. Immunol.* **9**, 1298 (2018).

41. Zhang, J. Yin and yang interplay of IFN-gamma in inflammation and autoimmune disease. *J. Clin. Invest.* **117**, 871–873 (2007).

42. Gauthier, M. et al. CCL5 is a potential bridge between type 1 and type 2 inflammation in asthma. *J. Allergy Clin. Immunol.* **152**, 94–106.e112 (2023).

43. Cano-Gamez, E. et al. Single-cell transcriptomics identifies an effectorness gradient shaping the response of CD4+ T cells to cytokines. *Nat. Commun.* **11**, 1801 (2020).

44. Salkowska, A. et al. Identification of novel molecular markers of human Th17 cells. *Cells* **9**, 1611 (2020).

45. Bao, K. & Reinhardt, R. L. The differential expression of IL-4 and IL-13 and its impact on type-2 immunity. *Cytokine* **75**, 25–37 (2015).

46. Zhang, J. Y. et al. Single-cell landscape of immunological responses in patients with COVID-19. *Nat. Immunol.* **21**, 1107–1118 (2020).

47. Siekmann, A. F. Biology of vascular mural cells. *Development* **150**, dev200271 (2023).

48. Yemisci, M. et al. Pericyte contraction induced by oxidative-nitrative stress impairs capillary reflow despite successful opening of an occluded cerebral artery. *Nat. Med.* **15**, 1031–1037 (2009).

49. Gonzales, A. L. et al. Contractile pericytes determine the direction of blood flow at capillary junctions. *Proc. Natl Acad. Sci. USA* **117**, 27022–27033 (2020).

50. Korte, N. et al. The Ca^{2+}-gated channel TMEM16A amplifies capillary pericyte contraction and reduces cerebral blood flow after ischemia. *J. Clin. Invest.* **132**, e154118 (2022).

51. Nayak, A. et al. Single-molecule analysis reveals that regulatory light chains fine-tune skeletal myosin II function. *J. Biol. Chem.* **295**, 7046–7059 (2020).

52. Jin, S. et al. Inference and analysis of cell-cell communication using CellChat. *Nat. Commun.* **12**, 1088 (2021).

53. Morrow, J. D., Parsons, W. G. 3rd & Roberts, L. J. Release of markedly increased quantities of prostaglandin D2 in vivo in humans following the administration of nicotinic acid. *Prostaglandins* **38**, 263–274 (1989).

54. Kong, D. & Yu, Y. Prostaglandin D_2 signaling and cardiovascular homeostasis. *J. Mol. Cell Cardiol.* **167**, 97–105 (2022).

55. Addor, F. A. Skin barrier in rosacea. *Bras. Dermatol.* **91**, 59–63 (2016).

56. Mylonas, A. et al. Type I IFNs link skin-associated dysbiotic commensal bacteria to pathogenic inflammation and angiogenesis in rosacea. *JCI Insight* **8**, e151846 (2023).

57. Holmes, A. D. Potential role of microorganisms in the pathogenesis of rosacea. *J. Am. Acad. Dermatol.* **69**, 1025–1032 (2013).

58. Moran, E. M., Foley, R. & Powell, F. C. Demodex and rosacea revisited. *Clin. Dermatol.* **35**, 195–200 (2017).

59. Bosch-Queralt, M., Fledrich, R. & Stassart, R. M. Schwann cell functions in peripheral nerve development and repair. *Neurobiol. Dis.* **176**, 105952 (2023).

60. Ydens, E. et al. The neuroinflammatory role of Schwann cells in disease. *Neurobiol. Dis.* **55**, 95–103 (2013).

61. Allard, D. E. et al. Schwann cell-derived periostin promotes auto-immune peripheral polyneuropathy via macrophage recruitment. *J. Clin. Invest.* **128**, 4727–4741 (2018).

62. Zhang, H. et al. Activated Schwann cells and increased inflammatory cytokines IL-1beta, IL-6, and TNF-alpha in patients' sural nerve are lack of tight relationship with specific sensory disturbances in Parkinson's disease. *CNS Neurosci. Ther.* **26**, 518–526 (2020).

63. Trias, E. et al. Schwann cells orchestrate peripheral nerve inflammation through the expression of CSF1, IL-34, and SCF in amyotrophic lateral sclerosis. *Glia* **68**, 1165–1181 (2020).

64. Buhl, T. et al. Molecular and morphological characterization of inflammatory infiltrate in rosacea reveals activation of Th1/Th17 pathways. *J. Invest. Dermatol.* **135**, 2198–2208 (2015).

65. Muto, Y. et al. Mast cells are key mediators of cathelicidin-initiated skin inflammation in rosacea. *J. Invest. Dermatol.* **134**, 2728–2736 (2014).

66. Mascarenhas, N. L., Wang, Z., Chang, Y. L. & Di Nardo, A. TRPV4 mediates mast cell activation in cathelicidin-induced rosacea inflammation. *J. Invest. Dermatol.* **137**, 972–975 (2017).

67. Wynn, T. A. & Barron, L. Macrophages: master regulators of inflammation and fibrosis. *Semin. Liver Dis.* **30**, 245–257 (2010).

68. Peng, Q. et al. mTORC1-mediated angiogenesis is required for the development of rosacea. *Front. Cell Dev. Biol.* **9**, 751785 (2021).

69. Basatemur, G. L., Jorgensen, H. F., Clarke, M. C. H., Bennett, M. R. & Mallat, Z. Vascular smooth muscle cells in atherosclerosis. *Nat. Rev. Cardiol.* **16**, 727–744 (2019).

70. Ma, F. et al. Single cell and spatial sequencing define processes by which keratinocytes and fibroblasts amplify inflammatory responses in psoriasis. *Nat. Commun.* **14**, 3455 (2023).

71. Hao, Y. et al. Integrated analysis of multimodal single-cell data. *Cell* **184**, 3573–3587.e3529 (2021).

72. Wu, T. et al. clusterProfiler 4.0: a universal enrichment tool for interpreting omics data. *Innovation* **2**, 100141 (2021).

Acknowledgements

Author contributions

J.L., Z.D., M.C., B.W. and Q.N. designed and conceived the study. Z.D., J.L., L.Y. and M.C. performed data analyses. L.Y., Z.D., P.Z. and S.J. performed scRNA-seq analysis. M.C. and Z.D. performed most experiments. Z.Z., W.X., W.S., D.J., B.W., F.L., Y.T., Y.H., Y.Z. contributed to sample collection. Z.W., Z.T., S.X., Y.Z. and M.W. helped to perform mouse experiments. H.X. provided critical discussion and suggestions. Z.D., J.L., L.Y., M.C., B.W. and Q.N. prepared the manuscript with input from coauthors.

Competing interests

The authors declare no competing interests.

Additional information